Materials Advances

ROYAL SOCIETY OF CHEMISTRY

PAPER

View Article Online
View Journal | View Issue

Cite this: *Mater. Adv.*, 2021, **2**, 1739

The role of the protein–water interface in dictating proton conduction across protein-based biopolymers

Yuval Agam, Ramesh Nandi, Tatiana Bulava and Nadav Amdursky *

Received 3rd December 2020,
Accepted 1st February 2021

DOI: 10.1039/d0ma00951b

rsc.li/materials-advances

Proton conducting polymers have become central in recent years, and especially for energy related applications. As such, unraveling their proton transport mechanism is of prime importance, specifically the different contribution of proton transport across bulk water inside the polymer *vs.* the transport at the interface between the polymer and water. In recent years, proton conducting biopolymers have been proven to be a green and sustainable alternative to traditional polymers. Unlike traditional synthetic polymers, the protein-based biopolymers that we use here can uptake a significant amount of water reaching 150 wt%, which might suggest a large contribution of bulk water proton transport *vs.* the protein–water interface one. We directly tackle the latter question and decipher the contribution of the protein–water interface in mediating proton conduction across our electrospun biopolymer by introducing two alternative experimental approaches. The first is to follow proton conduction across a highly aligned mat in parallel *vs.* perpendicular to the fiber direction, while the second is to measure proton conduction across a 'completely dry' network of the protein fibers. We conclude that although the protein-based mat contains a substantial amount of water, proton transport is mediated along the protein–water interface.

Introduction

Proton conducting materials have been the subject of numerous studies in recent years toward understanding their proton transport mechanism and their utilization in a variety of applications and especially energy-related ones, such as fuel cells, batteries, and capacitors. The commonly studied materials include metal–organic frameworks, solid acids, ceramic oxides, and synthetic polymers.[1–4] One of the challenges of this community, and specifically for proton conducting synthetic polymers, is to decipher the exact proton transport mechanism while distinguishing between the possible proton transport across bulk water and proton transport involving the polymeric backbone and its interface with water molecules. While going away from proton conducting materials, proton translocation across specific pathways is also a fundamental process in nature, whereas proteins are nature's choice as the proton mediating moiety, and mostly across a biological membrane. Inspired by nature, several recent works have utilized proteins for the formation of proton conducting materials.[5–9] Such bioinspired polymeric conductive materials are gaining momentum toward their integration in biomedical applications.[10,11] In addition to their applicative route, much effort was targeted toward deciphering how protons are being transported along such protein-based materials. Gorodetsky and coworkers formed drop-cast thin films out of a cephalopod structural protein that exhibit a relatively high proton conductivity of 0.1 mS cm^{-1} at room temperature and 90% relative humidity.[7] This performance is attributed to the large number of water molecules and the carboxylic acids in the protein structure. Ashkenasy and coworkers also demonstrated the importance of carboxylic acids in promoting proton conduction across self-assembled peptide fibrils.[12,13] Based on this knowledge, they recently showed a highly proton conducting peptide fibril network, which has merely 5–7 times lower conductivity than the Nafion® films.[6] The role of charged amino acids has also been proven to be essential in supporting very high proton conductivity across protein-based polymers.[5,9] Another example is the bovine serum albumin (BSA) protein that has been manipulated (by denaturing the protein) through the electrospinning process to receive a free-standing material with a fibrillar structure.[14] The main difference between the use of BSA and all the previously reported protein-/peptide-based materials is the sustainable nature of the BSA protein. Being one of the waste products of the bovine industry, the use of this protein for making new functional materials promotes a circular economy by using waste products. Furthermore, the protein can be

Schulich Faculty of Chemistry, Technion – Israel Institute of Technology, Haifa, 3200003, Israel. E-mail: amdursky@technion.ac.il

isolated in bulk quantities, resulting in a very low price-tag of the protein raw materials for the formation of the electrospun mats, and there is no need for any genetic expression or synthesis. We previously showed that after immersing the BSA mats in water, the hydrated mats could support proton conduction on a millimeter scale,[8] which can be disrupted using chemical modifications of the protein surface making them more hydrophobic.[15] Here, we wish to explore the role of water in mediating long-range proton conduction across the BSA mats, in comparison to the protein contribution. To do so, we use two different approaches: (1) using the fully hydrated BSA mat while controlling the matrix alignment; and (2) measuring proton conduction across a completely dry BSA thin fiber network as a function of relative humidity (RH). We show by several electrical measurements that the protein surface and its interface with water molecules are crucial for proton transport along the studied BSA electrospun system. We further compare our results to the 'more traditional' drop-casting technique of the BSA protein, thus emphasizing the role of the microstructure of the BSA electrospun fiber and its interface with water.

Results and discussion

Before diving into the results, it is of prime importance to distinguish the BSA electrospun system from other bioderived polymers. In all the reported proton-conducting protein-based polymers, the hydrated form of the polymer contained 12–20% water,[5,16] which corresponds also to the water uptake of proton-conducting polysaccharide-based biopolymers.[17–19] Importantly, no proton conduction has been observed for $<10\%$ water uptake for such polymers. Following the electrospinning process, the dry BSA mat contains just 4 wt% water,[8] however, upon immersing it in water, the BSA fibers act as a sponge, absorbing a vast amount of water, resulting in a staggering water uptake of 150 wt% for the hydrated BSA mat. Taking into consideration the substantial amount of water within the BSA mat, we wish to explore here the exact role of water in mediating long-range proton conduction across the BSA mats, in comparison to the protein contribution. This large number of water molecules within the BSA mat might well result in proton conduction solely across the bulk water within the mat in a Grotthuss-type proton diffusion process (Fig. 1, blue pathway). Another possibility is that proton transport takes place on the surface of the protein comprising the mat, in which both protonable side chains of amino acids (*i.e.*, which can participate in a hydrogen-bond network) as well as some water molecules at the surface of the protein are responsible for the proton diffusion (Fig. 1, red pathway).

Electrical measurements with fully hydrated and aligned BSA mats

In our first approach to decipher the role of water in proton conduction, we investigated how the matrix alignment can influence the proton conduction across the hydrated electrospun BSA mat by changing the protein matrix orientation from having a completely random network to having a well-aligned one. To create a randomly oriented free-standing BSA mat, we performed an electrospinning process using a pre-processed BSA protein (details in the Experimental section) with an aluminum collector.[8,14] Several studies reported the ability to control the matrix alignment during electrospinning of different polymers,[20] in which one of the straight forward methodologies to achieve such an alignment is by inducing a high insulating gap in the conductive collector.[21–23] As a result, the

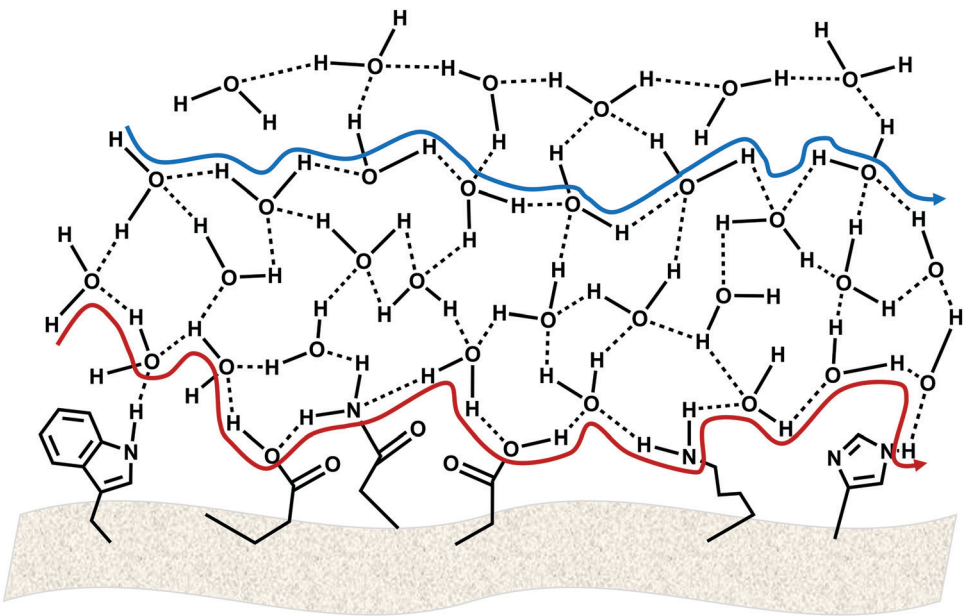

Fig. 1 Suggested pathways of proton diffusion *via* a Grotthuss-like mechanism. Blue pathway: proton diffusion solely *via* water molecules situated within the BSA mat. Red pathway: proton diffusion involving water molecules and functional groups on the surface of the protein fibers.

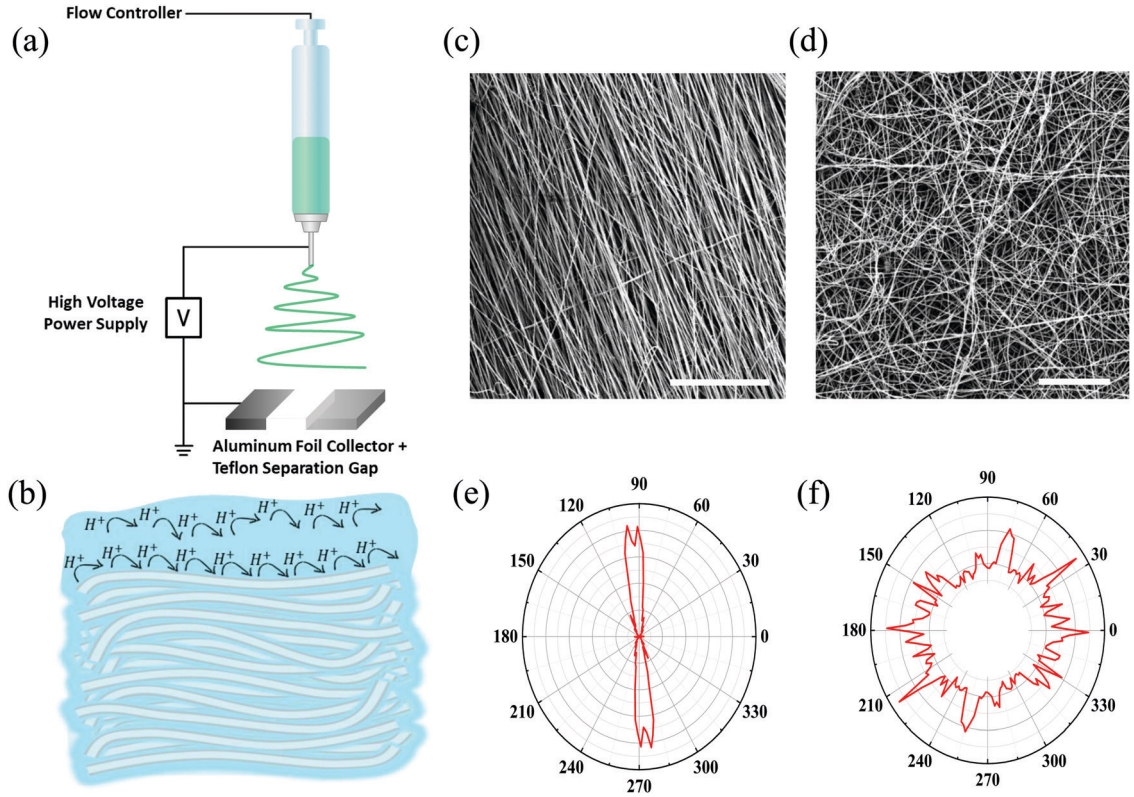

Fig. 2 (a) Schematic of the electrospinning setup. (b) Schematic of the BSA mat environment in the electrical measurements of this section, bringing into attention the large amount of water within the hydrated BSA mats, with suggested pathways of proton transport across bulk water *vs.* the protein–water interface. SEM images of the (c) aligned BSA mat, and (d) random oriented BSA mat. The scale in both images represents 100 μm. Fiber radial distribution calculated for the (e) aligned BSA mat, and (f) random oriented BSA mat.

applied electrostatic field induces the fibers to bridge between the conductive strips.[24] Here, we created fiber alignment by placing a strap of Teflon tape in the center of the aluminum foil collector (Fig. 2a). To date, few studies have addressed the effect of the matrix alignment on the conduction of electrospun materials,[25–29] all of them using synthetic polymers with moderate water content (<50%). As discussed, the water uptake of the BSA-based electrospun mat (150%) is exceptionally high. We hypothesize that if proton transport solely across the bulk water within the BSA electrospun mat is the predominant mechanism, we expect to observe no differences in the proton conductivity between the parallel and perpendicular orientations (or randomly distributed fibers) (Fig. 2b). Since the water portion of the hydrated BSA mat is significantly higher than the protein-content itself, it is fair to exclude the formation of discrete water channels within the protein polymer that might influence any differences between the measured conductances of the parallel and perpendicular orientations. On the other hand, if proton transport takes place along the protein interface with water (involving amino acid side chains), then we expect to see a higher proton transport efficiency for the parallel orientation as the percolating pathway along the fibers will be shorter in this orientation than in the perpendicular one (Fig. 2b).

To confirm the alignment of fibers and to explore their microstructure, we analyzed the scanning electron microscopy (SEM) images of the aligned mat (such as the one in Fig. 2c) in comparison to the SEM images of the randomly oriented mat (Fig. 2d). The images verify the generation of fiber alignment when using the modified collector. In terms of the microstructure of the aligned mat, it consists of fibers with a diameter of 1.58 ± 0.29 μm, which is in line with the fiber's diameter in the randomly oriented mat, albeit the fibers in the aligned mat are denser with the distance between fibers of around 1–3 μm. We used ImageJ software to determine the fiber radial distribution in both cases (Fig. 2e and f). As expected, the regular mat fibers do not show any preferred direction, while most of the aligned mat fibers order at the same angle. To explore the effect of the matrix alignment on the mat's ability to conduct protons we turned to electrochemical impedance spectroscopy (EIS) measurements. For this cause, we repeated the same measurement protocol used for the random BSA mat.[8] First, we soaked the aligned mat in purified water until full hydration. Next, we placed the mat on gold electrodes and dried away the excess of unbound water with tissue paper before measurement (in this stage, the mat contained ~150 wt% water). Each mat sample was measured in parallel and perpendicular to the fiber direction, simply by rotating the same sample of the aligned mat with respect to the electrodes. Fig. 3a displays the Nyquist plots (impedance imaginary part as a function of the impedance real part) of the aligned mat in both directions for different electrode separation distances. The curves show a semi-circle and a tail corresponding to the bulk proton conduction and the

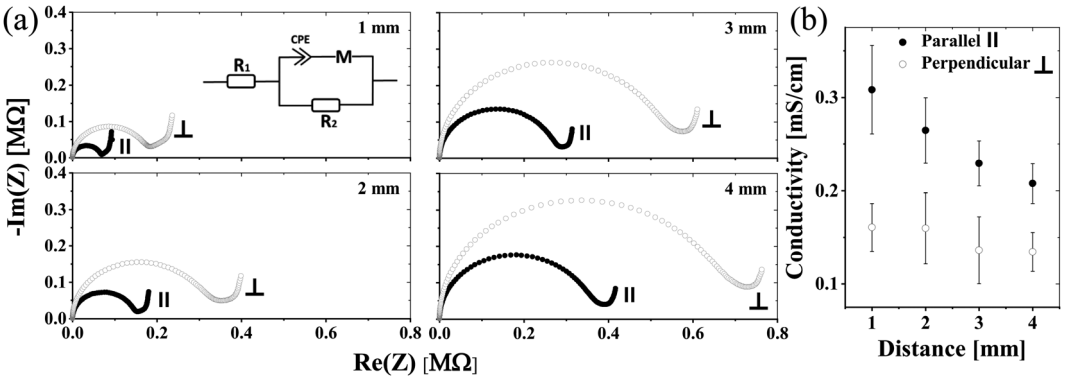

Fig. 3 (a) EIS Nyquist plots of the aligned BSA mat in parallel and perpendicular to the fiber orientations at different electrode separation distances, along with (b) the extracted conductivity values. The inset shows the equivalent circuit used to extract the resistance of the mats.

formation of a double-layer capacitance at the mat–electrode interface, respectively. This behavior is evidence of ionic conduction within blocking electrodes.[30] We extracted the mat resistance (R) from the EIS data by an equivalent circuit model[31] (Fig. 3a, inset). The conductivity (σ) was calculated considering the mat geometry using: $\sigma = \frac{l}{R \cdot A}$, where l is the electrode separation distance, and A is the cross sectional area (mat width times the mat thickness). Fig. 3b summarizes the mat conductivity in both directions for different electrode separation distances, showing that the mat conductivity in the fiber direction (parallel) is around two-fold higher than the conductivity perpendicular to the fibers, whereas the latter is in the same order of magnitude as the conductivity measured with a randomly oriented native BSA mat.[15] The higher conductivity of the mat, when measured in a specific direction, indicates the fundamental role of the protein interface in transporting protons through the material. The matrix alignment provides new favored percolating pathways for proton transport and thus enhances the conductivity in the fiber direction. However, this enhancement slowly diminishes as the distance between the electrodes becomes larger, suggesting that the preferred percolating pathway of the aligned BSA mat becomes less sustainable for very long distances. Interestingly, a similar change in conductivity between the parallel to the fiber orientation and the perpendicular one has been observed also for synthetic ionic conducting polymers with moderate water uptake, hence suggesting a similar proton transport mechanism albeit with a very different water content of the materials.[27,28]

Electrical measurements with a dry electrospun network of BSA fibers

While in the previous section we concluded that the protein–water interface has a fundamental role in supporting proton transport across our fully hydrated protein matrix (*i.e.*, containing bulk water), in this part we intend to directly confront the ability of the protein surface to mediate protons in a 'water-less' environment. To resolve this, we performed the electrospinning of the BSA fibers directly onto our electrodes (Fig. 4a), while making a layer of fiber network between the electrodes (the inset shows an optical microscopy image of the formed fiber network), meaning not a free-standing mat as before. Unlike the previous section, in which we used the hydrated (150 wt%) form of the BSA mat, we performed the electrical measurements in this section with the as-prepared dry state of the BSA fibers, containing merely 4 wt% of tightly bound water molecules to the protein structure,[8] while slowly increasing the RH values.[32] Importantly, this low water content is much lower than those of other reported protein-based polymers.[5,16] Our hypothesis in this section is that if proton transport across bulk water is the predominant proton conduction mechanism of the BSA mat, we should not detect any conductance of the dry network regardless of the RH, however, if the protein–water interface is the main proton transport relay, we should observe proton conduction even at low RH values which will be RH-dependent (Fig. 4b). Our EIS measurements of the formed layer at different RH levels (Fig. 4c) exhibited a semi-circle that is attributed to the conduction of the protons through the fibers. We determined the resistance values by applying the same equivalent circuit used for the aligned mat (Fig. 3a, inset). We observed a decrease in the extracted resistance values as a function of increasing relative humidity levels (Fig. 4c, inset). This behavior of elevated conduction upon increasing the RH levels is one of the hallmarks of proton conduction. We further examined the direct current (DC) electrical characteristics of the BSA thin layer. One major drawback of using the Au blocking electrode for measuring proton conduction is the proton accumulation near the surface of the electrode. Hence, we decided to use here palladium hydride (PdH) electrodes that can inject and accept protons, whereas for each proton injection, an electron will be transferred for the leads: $PdH \rightarrow Pd + H^+ + e^-$. In this way, protonic current transforms into a measurable electronic current,[7,17,18,33–36] resulting also in a significant reduction in the contact resistance between the PdH electrode and the (bio-)material.[37] Accordingly, we performed electrospinning of the BSA network layer directly onto palladium electrodes and measured the device I–V characteristics at room humidity (~80%) (Fig. 4d). As can be clearly seen in the figure, upon the exposure to hydrogen gas, the current

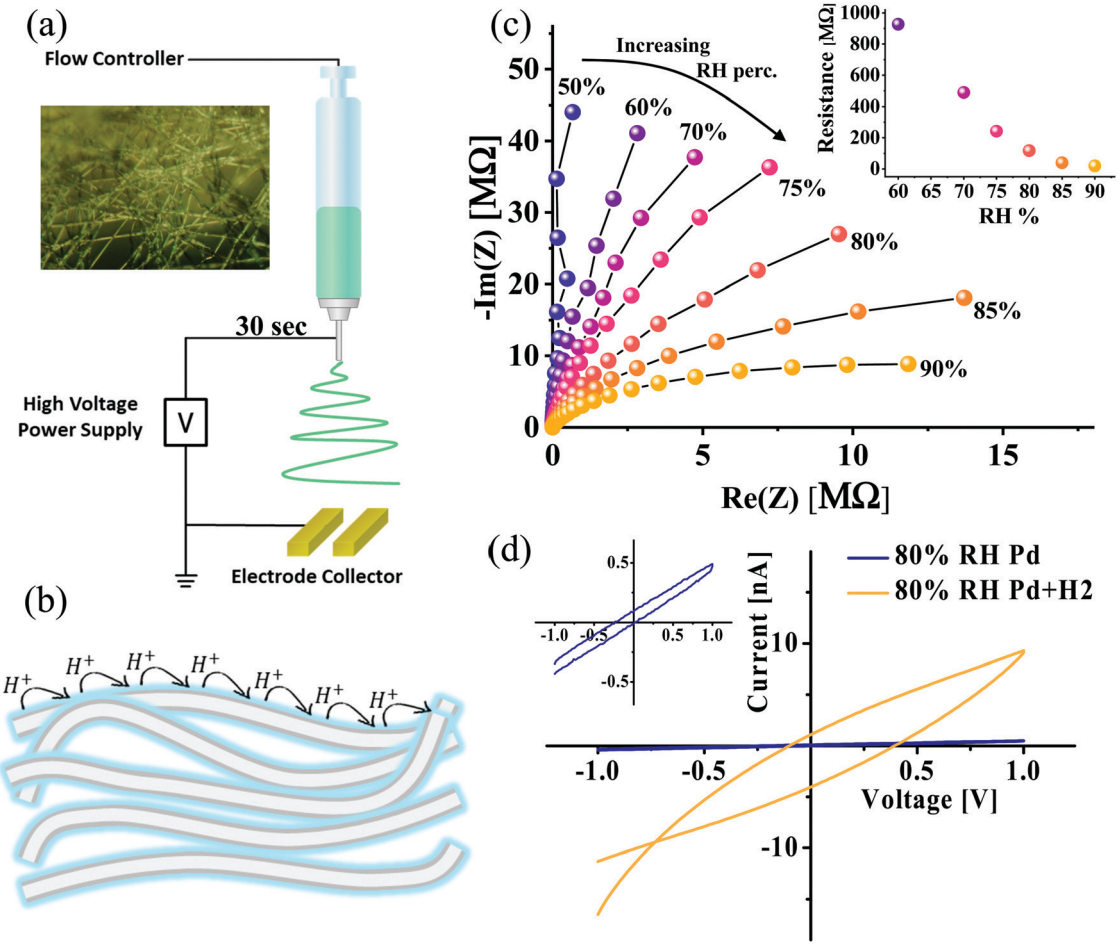

Fig. 4 (a) Schematic of the electrospinning setup. The inset shows an optical microscopy image of the BSA fiber monolayer. (b) Schematic of the BSA mat 'dry' environment in the electrical measurements of this section, emphasizing the RH-induced formation of the hydration shell around the BSA fibers, facilitating the proton transport on the surface of the protein fiber. (c) Nyquist plot of the BSA network layer at different RH levels. The inset shows the extracted resistance values as a function of RH. (d) Current–voltage characteristic of the BSA network layer on palladium-hydride electrodes. The inset shows a zoom-in of the curve before hydrogenating the Pd electrodes.

response increased by more than an order of magnitude, hence proving that protons are the charge carriers in the measured current. Overall, the different electrical setups and measurements in this section prove that a 'completely dry' protein-based material can mediate long-range proton conduction *via* the protein surface–water interface, meaning that water molecules improve the uniformity of the H-bond network on the surface of the protein (as displayed in Fig. 1).

Electrical measurements with a drop-cast BSA film

Until this point, we have established in our study here that the surface of the BSA fiber, formed in the electrospinning process, is important for mediating protons across our polymers. As mentioned in our introduction, several other proteins have shown proton mediating capabilities,[5,7,9] however, all of these works have used a drop-cast version of the proteins, meaning lacking a microstructure such as in our electrospun fibers. Accordingly, the last section of our study will serve as a control of comparing our results obtained with the BSA electrospun fibers to that obtained with a drop-cast BSA film (Fig. 5a) with similar geometrical parameters to our electrospun mat. Importantly, the drop-cast BSA films are not free-standing as the BSA mat, do not have a clear microstructure, and do not absorb a vast amount of water as the BSA electrospun mat. As shown in Fig. 5b, the measured resistance using EIS is highly RH-dependent, whereas at 90% RH, the calculated conductivity reaches a value of around 0.1 mS cm^{-1}, which is about 3 times lower than the conductivity measured with the aligned mat at the parallel configuration for the same distance between electrodes (1 mm). Nevertheless, the most important conclusion from this control experiment is the fundamentally different RH-dependency of the drop-cast BSA film (Fig. 5c) to the one measured with the network of the electrospun BSA fibers (Fig. 4c). While the decrease in resistance upon going from 60% to 90% RH is 40 fold for the electrospun BSA fibers, for the drop-cast BSA film, it is more than 3 orders of magnitude (~2700 folds) for the same range of RH%. This fundamental difference can be attributed to the microstructure of the electrospun BSA fibers, and accordingly the state of water molecules around it and the mode of proton transport (as

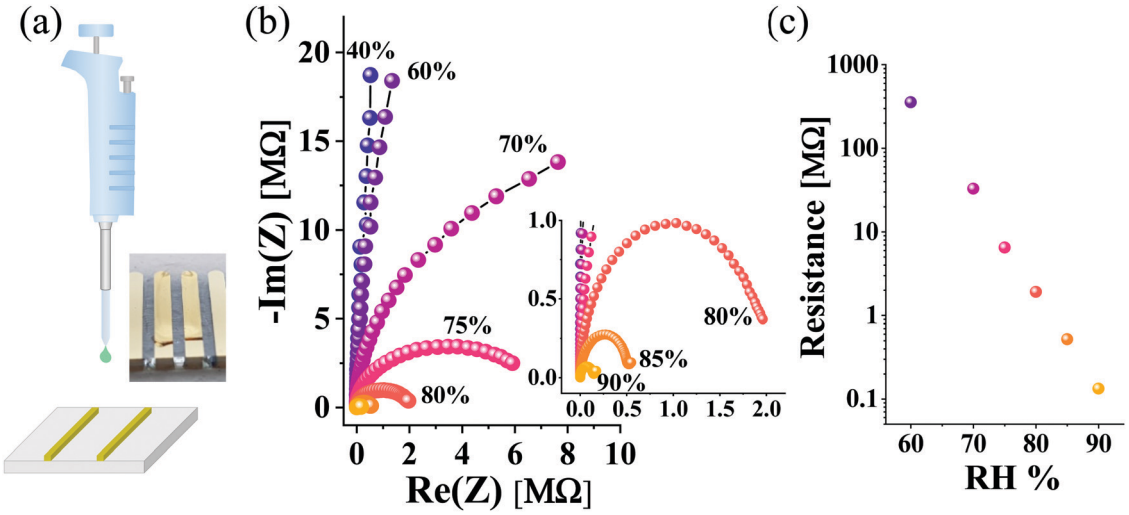

Fig. 5 (a) Schematic of the drop-casting process together with an image of the drop-cast film on the metallic electrodes. (b) Nyquist plot of the drop-cast BSA film at different relative humidity levels. The inset shows a zoom-in of the high RH values. (c) The extracted resistance values from the curves in (b) as a function of RH.

shown and discussed in Fig. 1). The surface of the BSA fiber is exposed to water molecules and can form an H-bond network between the amino acids on the surface of the BSA fiber and nearby water molecules. We have previously shown that these water states and H-bond network can be interrupted by introducing hydrophobicity onto the surface of the BSA fiber.[15] For the electrospun BSA fiber network, the rate-limiting step is the formation of a percolating H-bond pathway, consisting of water molecules and some amino acids of the protein capable of participating in this H-bond network. Hence, upon forming this network (as illustrated in the schematics of Fig. 4b), adding more water to the system by increasing RH results in a moderate decrease in resistance. On the other hand, for the drop-cast BSA film, there is no microstructure, and proton transport can be related to the formation of water channels, assisted by amino acids of the BSA protein. Accordingly, when more water molecules go into the film, they will significantly contribute to the proton conduction efficiency, resulting in the vast dependency of the measured resistance as a function of RH (Fig. 5c).

Concluding remarks

In this study, we investigated the proton conduction across electrospun BSA fibers, and specifically the role of the protein surface and its interface with water molecules in supporting such proton conduction. In the first part of our work, we investigated the effect of the fiber alignment on the fully hydrated (~150 wt%) mat conductivity, where we found that the parallel configuration of the aligned mat (compared to the electric field between the electrodes) is around 2-fold more conductive than the perpendicular orientation. This finding suggests that even in the fully hydrated mat, the protein surface and its interface with bulk water are crucial for the proton transport mechanism. In the second part of our study we directly examined if the presence of bulk water is necessary for proton conduction by removing water. To do so, we have used a dry network layer of the BSA electrospun fibers, *i.e.*, not a free-standing mat. We showed that this network can support some proton conductivity, which is RH-dependent, hence bulk water is not mandatory for the proton transport. We further proved that protons are indeed the main charge carriers by using proton-transparent hydrogenated Pd electrodes. We compared our results with the electrospun BSA fibers to that of a control sample of a drop-cast BSA layer. Unlike the BSA mat, a drop-cast BSA film is not free-standing and does not have any microstructure. We showed that the RH-dependency of the BSA drop-cast sample is fundamentally different than that of the electrospun BSA fibers, suggesting that while for the BSA electrospun fibers, the fiber-water interface is the predominant proton transport pathway, for the drop-cast sample, it is the water channel that supports proton conduction. All in all, the various electrical measurements used here to investigate the role of the protein–water interface in supporting proton conduction indicate that proton transport takes place at the protein interface with water and not in bulk water. As shown in our illustration in Fig. 1, and as suggested by the results obtained when using the dry BSA fiber network, to support the proton transport across the BSA fibers there is a need for a hydrogen bond network including both amino acid residues as well as some water molecules to bridge between them. Importantly, the 'dry' environment of the BSA fiber network has some resemblance to the local environment within natural proton transporting proteins, such as the transmembrane proton shuttling protein transporters. It is well understood that proton transport within these proteins involves both water molecules and amino acids that can participate in hydrogen bonding, and especially glutamic and aspartic acids.[38] However, while in the biological system, this mode of proton transport takes place for very short distances of <5 nm, and

usually across a membrane, we show that it can support very long proton transport on the millimeter scale. Outside of the biological world, the role of the proton transport mechanism, and the involvement of bulk water in it, is a vivid line of research in the wide field of proton conducting polymers and ionomers. Accordingly, our new findings on the role of the interface between the proton conducting (bio-)polymer and water in supporting proton conduction can shed some light on the general proton transport mechanism of various proton-conducting polymers.

Experimental section

Electrospinning of BSA mats

Electrospinning solution was prepared by dissolving BSA (MP Biomedicals) in 90% 2,2,2-trifluoroethanol (Apollo Scientific) for a final BSA concentration of 14% (w/v). After 12 hours, 5% (v/v) β-mercaptoethanol (Alfa Aesar) was added and the solution was continuously stirred for 3 h. Electrospinning was performed in a custom-built system with a ground aluminum collector (for the random oriented mat). A 15 kV bias was applied on a 24-gauge blunt needle with an injection rate of 1.5 ml h^{-1}. The needle was fixed 12 cm above the collector. For the randomly oriented mat, the spinning was directly onto the aluminum collector, and the final mat thickness was around 60 μm. To create the aligned mat, a strap of Teflon tape was placed in the middle of the aluminum collector, and in this configuration, the final thickness of the aligned mat was thinner and around 30 μm. The latter thickness of the aligned mat is an upper limit as thicker mats in this configuration will lose the effect of the Teflon tape induced orientation of the electric field, and will result in a randomized orientation above this thickness.

Metal finger electrode fabrication

Heavily p-doped silicon wafers with a SiO_2 dielectric layer (110 nm) and glass microscope slides were used as substrates for the devices used in the DC and impedance measurements, respectively. The substrate was sonicated for 5 min in the following series of solvents: acetone followed by methanol, isopropanol, and finally ethanol. After the last sonication, silicon substrates were washed with distilled water, and dried on a glass Petri dish heated to 120 °C. Glass substrates were washed with distilled water and dried using hot air. Using an E-beam evaporator at a deposition rate of 2 Å s^{-1} under 5×10^{-7} Torr at room temperature, 100 nm Au/Pd on 10 nm Cr were evaporated through shadow masks. Mats were placed on finger electrodes and gently dried with filter paper to remove excess water. The water weight percentage within the BSA mat in all electrical experiments was around 150 wt%.

Electrospinning of the BSA thin layer network

A similar solution has been used as described above. A 15 kV bias was applied on a 24-gauge blunt needle, 12 cm above the collector, with an injection rate of 1.5 ml h^{-1} for 30 seconds. The BSA network was formed on Au electrodes with an inter-electrode distance of 1 mm and 2 cm width and Pd electrodes with an inter-electrode distance of 100 μm and 2.7 cm width.

Impedance measurements

Impedance measurements were performed using an MTZ-35 impedance/gain-phase analyzer (Bio-Logic). The gold electrodes were contacted using a probe station micromanipulator (TP102SV-PS, INSTEC). A 50 mV AC bias was applied during the measurements without DC bias. The frequency range of 10 MHz to 10 Hz was used. Humidity dependence was studied inside the probe station using a custom-built gas system, where N_2 gas was passed through water to control the humidity.

DC current–voltage measurements

DC current–voltage measurements were performed using a source measure unit (B2901A, Keysight). A BSA thin layer network was deposited on Pd finger electrodes with a distance of 100 μm between electrodes, which were placed inside a probe station (TP102SV-PS, INSTEC). The palladium electrodes were contacted using the probe station micromanipulator. The current was measured as a function of voltage in the range of −1 V to 1 V. To perform palladium hydride measurements, hydrogen gas was injected into the chamber for 30 minutes.

Drop cast BSA film

The film was prepared by drop-casting 10% (w/v) BSA aqueous solution onto a gold finger electrode with an electrode separation distance of 1 mm. The layer was then dried in air for 12 hours to form a film. The final film thickness was around 30–40 μm.

Conflicts of interest

The authors declare no conflicts of interest.

Acknowledgements

N. A. thanks the Binational Science Foundation (grant number 2018239), the Ministry of Science and Technology (grant numbers 3-16243 and 3-16312), and the PhosAgro/UNESCO/IUPAC grant in green chemistry (number 4500378239) for financial support. We thank the Russel Berrie Nanotechnology Institute (RBNI) and the Grand Technion Energy Program (GTEP) for their support in equipment use.

References

1 B. Li, H. M. Wen, Y. Cui, W. Zhou, G. Qian and B. Chen, *Adv. Mater.*, 2016, **28**, 8819–8860.
2 S. M. Haile, D. A. Boysen, C. R. I. Chisholm and R. B. Merie, *Nature*, 2001, **410**, 910–913.
3 Z. Tao, L. Yan, J. Qiao, B. Wang, L. Zhang and J. Zhang, *Prog. Mater. Sci.*, 2015, **74**, 1–50.
4 M. B. Karimi, F. Mohammadi and K. Hooshyari, *Int. J. Hydrogen Energy*, 2019, **44**, 28919–28938.

5 A. Pena-Francesch, H. Jung, M. A. Hickner, M. Tyagi, B. D. Allen and M. C. Demirel, *Chem. Mater.*, 2018, **30**, 898–905.
6 O. Silberbush, M. Engel, I. Sivron, S. Roy and N. Ashkenasy, *J. Phys. Chem. B*, 2019, **123**, 9882–9888.
7 D. D. Ordinario, L. Phan, W. G. Walkup IV, J.-M. Jocson, E. Karshalev, N. Hüsken and A. A. Gorodetsky, *Nat. Chem.*, 2014, **6**, 596–602.
8 N. Amdursky, X. Wang, P. Meredith, D. D. C. Bradley and M. M. Stevens, *Adv. Mater.*, 2016, **28**, 2692–2698.
9 C. Ma, J. Dong, M. Viviani, I. Tulini, N. Pontillo, S. Maity, Y. Zhou, W. H. Roos, K. Liu, A. Herrmann and G. Portale, *Sci. Adv.*, 2020, **6**, eabc0810.
10 A. Burnstine-Townley, Y. Eshel and N. Amdursky, *Adv. Funct. Mater.*, 2020, **30**, 1901369.
11 N. Amdursky, E. D. Głowacki and P. Meredith, *Adv. Mater.*, 2019, **31**, 1802221.
12 O. Silberbush, M. Amit, S. Roy and N. Ashkenasy, *Adv. Funct. Mater.*, 2017, **27**, 1604624.
13 J. Lerner Yardeni, M. Amit, G. Ashkenasy and N. Ashkenasy, *Nanoscale*, 2016, **8**, 2358–2366.
14 Y. Dror, T. Ziv, V. Makarov, H. Wolf, A. Admon and E. Zussman, *Biomacromolecules*, 2008, **9**, 2749–2754.
15 S. Mondal, Y. Agam, R. Nandi and N. Amdursky, *Chem. Sci.*, 2020, **11**, 3547–3556.
16 D. D. Ordinario, L. Phan, Y. Van Dyke, T. Nguyen, A. G. Smith, M. Nguyen, N. M. Mofid, M. K. Dao and A. A. Gorodetsky, *Chem. Mater.*, 2016, **28**, 3703–3710.
17 Y. Deng, E. Josberger, J. Jin, A. F. Rousdari, B. A. Helms, C. Zhong, M. P. Anantram and M. Rolandi, *Sci. Rep.*, 2013, **3**, 2481.
18 C. Zhong, Y. Deng, A. F. Roudsari, A. Kapetanovic, M. P. Anantram and M. Rolandi, *Nat. Commun.*, 2011, **2**, 1–5.
19 J. Wünsche, Y. Deng, P. Kumar, E. Di Mauro, E. Josberger, J. Sayago, A. Pezzella, F. Soavi, F. Cicoira, M. Rolandi and C. Santato, *Chem. Mater.*, 2015, **27**, 436–442.
20 W. E. Teo and S. Ramakrishna, *Nanotechnology*, 2006, **17**, R89.
21 H. Yuan, Q. Zhou and Y. Zhang, *Electrospun Nanofibers*, 2017, 125–147.
22 T. Aubert, L. Palangetic, M. Mohammadimasoudi, K. Neyts, J. Beeckman, C. Clasen and Z. Hens, *ACS Photonics*, 2015, **2**, 583–588.
23 D. Li, Y. Wang and Y. Xia, *Adv. Mater.*, 2004, **16**, 361–366.
24 D. Li, Y. Wang and Y. Xia, *Nano Lett.*, 2003, **3**, 1167–1171.
25 A. Yang, Z. Huang, G. Yin and X. Pu, *Colloids Surf., B*, 2015, **134**, 469–474.
26 J. Wang, P. Li, Y. Zhang, Y. Liu, W. Wu and J. Liu, *J. Membr. Sci.*, 2019, **585**, 157–165.
27 T. Tamura, R. Takemori and H. Kawakami, *J. Power Sources*, 2012, **217**, 135–141.
28 T. Ibaraki, M. Tanaka and H. Kawakami, *Electrochim. Acta*, 2019, **296**, 1042–1048.
29 X. Gong, G. He, Y. Wu, S. Zhang, B. Chen, Y. Dai and X. Wu, *J. Power Sources*, 2017, **358**, 134–141.
30 R. A. Huggins, *Ionics*, 2002, **8**, 300–313.
31 M. Sheliakina, A. B. Mostert and P. Meredith, *Adv. Funct. Mater.*, 2018, **28**, 1805514.
32 Due to the huge amount of water in the hydrated BSA mat configuration, there is no meaning for a RH-dependent electrical measurement study with the fully hydrated mat.
33 D. D. Ordinario, L. Phan, J. M. Jocson, T. Nguyen and A. A. Gorodetsky, *APL Mater.*, 2015, **3**, 1–6.
34 H. A. Patel, J. Selberg, D. Salah, H. Chen, Y. Liao, S. K. Mohan Nalluri, O. K. Farha, R. Q. Snurr, M. Rolandi and J. F. Stoddart, *ACS Appl. Mater. Interfaces*, 2018, **10**, 25303–25310.
35 J. Selberg, M. Jia and M. Rolandi, *PLoS One*, 2019, **14**, e0202713.
36 E. E. Josberger, P. Hassanzadeh, Y. Deng, J. Sohn, M. J. Rego, C. T. Amemiya and M. Rolandi, *Sci. Adv.*, 2016, **2**, 1–7.
37 J. T. Robinson, J. J. Pietron, B. Blue, F. K. Perkins, E. Josberger, Y. Deng and M. Rolandi, *J. Mater. Chem. C*, 2017, **5**, 11083–11091.
38 T. E. Decoursey, *Physiol. Rev.*, 2003, **83**, 475–579.